RSC Advances

ROYAL SOCIETY OF CHEMISTRY

www.rsc.org/advances

Microwave-assisted preparation of sepiolite-supported magnetite nanoparticles and its removal ability to low concentration Cr(VI)

Sheng-Hui Yu[1)], Han-Li[1)], Qi-Zhi Yao[2)], Sheng-Quan Fu[3)], Gen-Tao Zhou[1)] *

[1] CAS Key Laboratory of Crust-Mantle Materials and Environments, School of Earth and Space Sciences, University of Science and Technology of China, Hefei 230026, P. R. China.

[2] School of Chemistry and Materials Science, University of Science and Technology of China, Hefei 230026, P. R. China.

[3] Hefei National Laboratory for Physical Sciences at Microscale, University of Science and Technology of China, Hefei 230026, P. R. China.

Corresponding author: Prof. Dr. Gen-Tao Zhou

Tel.: 86 551 63600533

Fax: 86 551 63600533

Email: gtzhou@ustc.edu.cn

Abstract

Sepiolite-supported magnetite nanoparticles (SSMNPs) were successfully prepared by a facile, robust and time-saving microwave-assisted method. The SSMNPs were characterized by a wide range of techniques including powder X-ray diffraction (XRD), field emission scanning electron microscopy (FESEM), transmission electron microscopy (TEM), energy dispersive X-ray spectroscopy (EDX), X-ray photoelectron spectra (XPS), and Brunauer-Emmett-Teller (BET) gas sorptometry. It was found that the sepiolite-supported magnetite nanoparticles show better dispersion and less aggregation than their counterparts obtained by common heat method. Moreover, the removal ability of SSMNPs to Cr(VI) was investigated systematically. The SSMNPs exhibit excellent removal ability to low concentration Cr(VI), and its removal capacity is 33.4 mg/g (per unit mass of magnetite) at pH 3.0 and adsorbent concentration 1.0 g/L, higher than that of the unsupported magnetite nanoparticles (22 mg/g). The adsorption data fit well with the Redlich-Peterson isotherm model. Due to the simplicity of the synthetic procedure, the high removal efficiency for Cr(VI) and less remain of Fe^{3+} in the treated solution, as well as easy separation of the adsorbent with water, the sepiolite-supported magnetite nanoparticles have quite real potential for applications in water treatment.

Keywords: Sepiolite; Magnetite nanoparticles; Microwave-assisted method; Hexavalent chromium; Removal of heavy metal ion

1. Introduction

Hexavalent chromium, Cr(VI), usually exists in wastewater as oxyanions such as chromate (CrO_4^{2-}), hydrochromate ($HCrO_4^-$) and dichromate ($Cr_2O_7^{2-}$), depending on pH and concentration of the chromium solution, and does not precipitate easily using conventional precipitation methods compared with trivalent chromium Cr(III).[1,2] Cr(VI) is highly toxic agents that act as carcinogens, mutagens, and teratogens in biological systems.[3,4] The chromium pollution arises mainly from the industries involved in mining, leather tanning, cement, dye, electroplating, steel, metal alloys, photographic material and metal corrosion inhibition.[5] To reduce human exposure to chromium, the US Environmental Protection Agency (EPA) has set a maximum contaminant level (MCL) of 0.1 mg/L for total chromium in drinking water.[3] The removal of Cr(VI) from industrial waste is well needed all over the world.[6] A variety of methods have been developed for the removal of chromium compounds from industrial wastewater. For high concentration Cr(VI)-containing wastewater, chemical reduction, followed by precipitation is the most widely used technique.[6] When dealing with Cr(VI)-containing wastewater at low to mid concentration (10-200 mg/L), the use of biological method is regarded as a promising technology.[7] However, the treatment of low concentration Cr(VI)-containing wastewater (1-10 mg/L) is still a challenge in practical application, and the adsorption by nanoadsorbents is considered as the most suitable route.[8]

Since the solubility, mobility, and toxicity of chromium depend on its oxidation state, redox reactions involving Cr are extremely important in determining its fate in the environment and potential risk to human health.[9] Many studies have demonstrated that ferrous iron [Fe(II)] is an important reductant of Cr(VI) in natural environments,[10,11] and magnetite is one of the Fe(II)-containing minerals, having the potential to reduce and immobilize Cr(VI).[12] Reduction of Cr(VI), Tc(VII), U(VI), and Hg(II) by structural Fe(II) in magnetite has been investigated under various environmental conditions, and a coupled reduction sorption process was proposed as the most mechanism.[13-16] Previous studies show that the removal capacity and reactivity for pollutants of the popular iron-based magnetic nanoparticles, namely nano zero-valent iron (nZVI), magnetite (Fe_3O_4) and maghemite (γ-Fe_2O_3)

nanoparticles, are highly size dependent.[17,18] For example, Shen et al. reported that the removal capacity for Cr(VI) of Fe_3O_4 nanoparticles (8 nm) was about seven times higher than that of coarse-grained counterparts (50 μm).[19] However, it has been found that the smaller the nanoparticles are, the higher tendency of aggregation stemming from a high surface free energy. And the magnetism of iron-based magnetic nanoparticles would enhance the aggregation of nanoparticles. The formation of aggregates could decrease the surface area of the magnetic nanoparticles, thereby limiting the treatment performance for contaminants.[20] Moreover, the application of nanoparticles for environmental treatment deliberately injects or dumps engineered nanoparticles into the soil or aquatic systems. This has resultantly attracted increasing concern from all stakeholders. The advantages of magnetic nanoparticles (especially for nZVI) such as their small size, high reactivity and great capacity, could become potential lethal factors by inducing adverse cellular toxic and harmful effects.[21] Therefore, to effectively apply magnetic nanoparticles in wastewater treatments, it is essential to balance effects on their reactivity, capacity, reusability and biocompatibility.[22]

Recently, numerous technologies have been developed using porous materials as mechanical supports to enhance the dispersibility of magnetic nanoparticles. For example, resin-supported nZVI particles were used to remove Cr(VI) and Pb(II) from aqueous solutions where reaction rates of the removal for Cr(VI) and Pb(II) were enhanced by 5 and 18 fold, respectively.[23] Black carbon-supported nZVI also showed high removal efficiency for Cr(VI) compared with unsupported nZVI.[24] Nanoscale iron particles decorated on graphene sheets showed enhanced Cr(VI) adsorption capacity compared with bare iron nanoparticles.[25] Clay minerals have raised up much interest among researchers in recent years, owing to their high specific surface area with unique swelling, intercalation, and ion-exchange properties, low cost and ubiquitous presence in most soils, and also been reported as support materials for magnetic nanoparticles. For example, nZVI was supported on a pillared bentonite (Al-bent) to enhance the reactivity of nZVI and prevent its aggregation. And the removal efficiency for Cr(VI) was not only much higher than that by nZVI, but also superior to the sum of nZVI reduction and Al-bent adsorption.[26] The presence of kaolinite during the synthesis of iron nanoparticles led to a partial decrease in their extent of aggregation, producing dispersed nanoparticles with sizes varying between 10 and 80 nm, and the dispersed ZVI nanoparticles

demonstrated high uptake capacities toward Cu^{2+} and Co^{2+}.[27] Diatomite and montmorillonite-supported magnetite nanoparticles exhibited a higher adsorption capacity for Cr(VI) per unit mass of magnetite than the unsupported nanoscale magnetite, due to the better dispersing and less coaggregation.[28,29] However, seeking new support materials and more facile synthesized methods in the fabrication of supported magnetic nanoparticles is still of great concern to researchers in the fields of materials and environmental sciences.

Sepiolite is a non-swelling, lightweight, porous, fibrous clay with a large specific surface area, and has an Orthorhombic structure with space group P*nna*. It shows an alternation of blocks and tunnels that grow up in the fiber direction, i.e., its crystallographic [100] direction. Each structural block is built by two tetrahedral silica sheets with a central magnesia sheet. Differing from other 2:1 silicates, the silica sheets are discontinuous, giving rise to the formation of structural tunnels. The high surface area and porosity, unusual needle-like morphology, silanol-based chemistry of the surface as well as high chemical and mechanical stability of this clay make it a valuable material,[30-32] and has been widely used to remove undesired components from household and industrial wastewaters or as catalyst support for Ag, TiO_2, ZnO and CuO in the photocatalytic treatment.[33-39] Lately, Fe_3O_4/sepiolite magnetic composite was also prepared by a chemical co-precipitation method with careful control of temperature and pH of the reaction medium, and was used as adsorbent for the removal of atrazine from aqueous solution.[40,41]

Since the microwave-assisted method was first reported in 1986,[42,43] the use of MW energy in chemical reactions has been recognized as much faster, cleaner, and more economical than the conventional methods due to its dielectric volumetric heating.[44] A variety of materials such as carbides, nitrides, complex oxides, silicides, zeolites, apatite, various alloys, etc. have been synthesized using microwave-assisted method.[45] With the assistance of microwave-irradiation, our group has successfully prepared hierarchical nanospheres of ZnS, flower-like β-FeSe microstructures, various hierarchical nanostructures of copper sulfide, monodisperse pyrite microspherolites.[46-49] Noteworthy, however, the report on the fabrication of clay-supported materials by microwave-assisted method is still scarce.

Herein, SSMNPs with excellent dispersity are successfully prepared by a routine microwave-assisted co-precipitation of Fe^{2+}, Fe^{3+} in the mixed solvent of water and EG, and

the removal ability of the SSMNPs to Cr(VI) is evaluated systematically.

2. Experimental Section

2.1 Materials and chemicals.

All the chemicals were used as purchased without further purification. Iron(III) chloride hexahydrate ($FeCl_3.6H_2O$), iron(II) chloride tetrahydrate ($FeCl_2.4H_2O$), ethanol (EtOH), ethylene glycol (EG) and sodium hydroxide (NaOH) were purchased from Sinopharm Chemical Reagent Co., Ltd, Sepiolite was purchased by Sigma-Aldrich Chemical Reagent Co., Ltd. Distilled water was used in all preparations. A microwave-reflux synthesis system (WBFY-201, Yuhua, Gongyi, China), with cycle period of 22 seconds, output power of 800 W, working frequency of 2.45×10^9 Hz, was used for the preparation of sepiolite-supported magnetite and unsupported magnetite nanoparticles. The microwave reactor could operate at 10%, 30%, 50%, 80%, and 100% of full power by changing the on/off duration of the microwave irradiation on cycle model.

2.2 Synthesis of sepiolite-supported and unsupported magnetite nanoparticles

The sepiolite-supported and unsupported magnetite nanoparticles were prepared using a one-pot microwave-assisted co-precipitation of ferric and ferrous ions with or without sepiolite as support material, respectively. The typical synthesis process was as follows: 0.27 g (1 mmol) of $FeCl_3\cdot6H_2O$ and 0.10 g (0.5 mmol) of $FeCl_2.4H_2O$ were dissolved in 20 mL of ethylene glycol in a 100 mL round-bottomed flask by ultrasonication for a few minutes, and then 0.25 g of white raw sepiolite was dispersed in the solution under ultrasonication. Subsequently, a 5 mL of NaOH (0.16 g, 4 mmol) solution was also introduced into the solution with ultrasonication, and the pH of the solution was measured to be 11.5. The round-bottomed flask with the reactants was equipped on the microwave reactor, and purged for a few minutes with nitrogen prior to the turning on of the microwave reactor. After 20 min microwave irradiation at 80% of the full power under nitrogen flow, the round-bottomed flask was naturally cooled down to room temperature. It was found that a black product was formed. The product was collected by centrifugation and washed with deionized water and ethanol,

and finally dried at 50 ^{o}C under vacuum, which was designated as sample SSM-1. Magnetite nanoparticles prepared under the same experimental conditions without sepiolite were designated as sample MNPs. For comparison, different amounts of sepiolite (0.50 and 0.125 g) were used to obtain SSMNPs with different magnetite loading by the same procedures. The obtained samples were labeled as samples SSM-2 and SSM-3, respectively. The loading of magnetite in the modified sepiolite is determined by an inductively coupled plasma atomic emission spectroscopy (ICP-AES, optima 7300 DV), and corresponding results are listed in Table 1.

2.3 Characterizations.

Several analytical techniques were used to characterize the synthesized products. The powder X-ray diffraction (XRD) patterns of as-synthesized samples were recorded with a Japan MapAHF X-ray diffractometer equipped with graphite-monochromatized Cu Kα irradiation (λ = 0.154056 nm). The morphology and microstructure of the samples were observed with a JEOL JSM-2010 field-emission scanning electron microscope (FESEM). Transmission electron microscopy (TEM) images were obtained on a Hitachi model H-800 transmission electron microscope with an accelerating voltage of 200 kV. Energy-dispersive X-ray spectroscopy (EDX) analyses were obtained with an EDAX detector installed on the same TEM. X-ray photoelectron spectra (XPS) were taken on a Thermo ESCALAB 250 X-ray photoelectron spectrometer with Al Kα radiation. Nitrogen sorption data was performed at a Micromeritics Tristar II 3020M automated gas adsorption analyzer utilizing Barrett-Emmett-Teller (BET) calculations for surface area and Barrett-Joyner-Halenda (BJH) calculations for pore size distribution for the adsorption branch of the isotherm.

2.4 Removal experiments

A stock solution containing hexavalent chromium was prepared by dissolving $K_2Cr_2O_7$ with deionized water and a series of solutions used during the experiment were prepared by diluting the stock to the desired concentrations-actual concentrations were measured using ICP-AES. In a typical removal run, 50 mg of adsorbent was added into 50 mL of solution containing 2×10^{-5} mol/L (ca. 1.0 mg/L) Cr(VI). The mixture was adjusted to pH 3.0 $\pm$ 0.1 by 0.1 M HCl and 0.1 M NaOH solution and stirred for 24 h at room temperature (293 K). The SSMNPs with absorbed Cr was first separated from the mixture with a permanent hand-held

magnet, and then by centrifugation at 10000 rpm for 10 min. After that, the supernatant was filtered using a 0.2 μm pore size membrane filter. The residual Cr in the solution was first determined by ICP-AES. Inductively coupled plasma mass spectrometry (ICP-MS, Plasma Quad3) was used when the concentration of Cr is below 0.1 mg/L. The effects of pH, contact time, adsorbent dosage, initial concentration of Cr(VI), magnetite loading on the removal of Cr(VI) as well as the reusability of the adsorbent were investigated by the same procedures. Furthermore, in order to evaluate the role of sepiolite and magnetite nanoparticles in the hybrid system, their removal abilities to Cr(VI) and Cr(III) were systematically tested, respectively. All adsorption studies were repeated in duplicate, and averaged values were reported. The amount of chromium adsorbed at equilibrium, q_e (mg/g), uptake percentage U%, were calculated according to the following equations, respectively:

$$q_e = \frac{(C_o - C_e) \times V}{W}$$

$$U\% = \frac{(C_o - C_t) \times 100\%}{C_o}$$

where C_o (mg/L), C_t (mg/L) and C_e are the liquid phase concentration of the chromium at initial, any time t and equilibrium, respectively. V is the volume of the solution (mL) and W is the mass of the adsorbent added (mg). The adsorption isotherms were analyzed by Langmuir model (eq. 1), Freundlich model (eq. 2), and Redlich-Peterson model (eq. 3), respectively.[50]

$$q_e = \frac{K_L b C_e}{(1 + b C_e)} \quad (1)$$

$$q_e = K_F C_e^{1/n} \quad (2)$$

$$q_e = \frac{K_R C_e}{1 + a_R C_e} \quad (3)$$

where q_e (mg/g) is the equilibrium sorption capacity, C_e (mg/L) is the equilibrium sorbate concentration in solution, K_L and b are the Lagmuir constants related to adsorption capacity and energy of adsorption, respectively. K_F (mg/g(L/mg)1/n) is a Freundlich constant, 1/n is an empirical constant, which indicates the intensity of the adsorption. K_R (L/g) and a_R (L/mg) are Redlich-Peterson isotherm constants, and β is the exponent, which lies between 1 and 0. If β = 1, the Langmuir is preferable isotherm; if β = 0, the Freundlich is preferable isotherm.

3. Results and Discussion

3.1 Characterization of the sepiolite-supported magnetite nanoparticles

The morphology textures of sepiolite before and after modification were observed by SEM and TEM. The raw sepiolite is a typical fibrous nanomineral with the length of several micrometers and the width of ca. 50 nm (Figure 1a). After sepiolite was modified, the white sepiolite turns into black, and the black sepiolite shows obvious magnetic property (Figure 1b inset A). Compared with the SEM image of raw sepiolite (Figure 1a), the modified sepiolite almost exhibits intact morphological characteristics after a 30 min irradiation in the Fe^{2+}/Fe^{3+} solution, but massive nanoparticles can be clearly observed on the surface of sepiolite fibers. The EDX spectrum shows that the rod-like structures contain the elements of O, Si, Mg, Fe, indicating the formation of iron oxides-sepiolite composite (e.g., Figure 1b inset B). The higher-magnification SEM image of the modified sepiolite (Figure 1c) shows that nanoparticles stick on the sepiolite surface and no obvious aggregates of the nanoparticles are observed. The hybrid structures are further confirmed by TEM analysis. Figure 1d shows that even after a few minutes of ultrasonic irradiation, the nanoparticles still anchor to the surface of sepiolite, and no separated individuals or aggregates of the nanoparticles can be found, demonstrating the strong affiliation between the nanoparticles and sepiolite. The high resolution TEM analyses reveal that the average size of the nanoparticles is ca.10 nm (e.g., Figure 1d inset).

XRD patterns of raw sepiolite and the modified sepiolite are presented in Figure 2a. Raw sepiolite shows a typical XRD powder diagram of pure sepiolite (JCPDF: 13-0595) with a characteristic reflection at d_{110} = 12.0 Å, corresponding to the interlayer distance in the sepiolite structure.[51] The XRD pattern of modified sepiolite has also nearly no changes compared with raw sepiolite, indicating that sepiolite is stable even under strong microwave irradiation. Nevertheless, after carefully compared, one can still find that the diffraction peaks near $2\theta = 35.5^{o}$ (the strongest diffraction peak of magnetite located)[52] in the XRD pattern of modified sepiolite become more strong and broad, which may indicate the formation of

magnetite nanoparticles, as highlighted by a blue circle in Figure 2a. Because γ-Fe_2O_3 and Fe_3O_4 have the same inverse spinel structure and similar lattice parameters, the phase of magnetite couldn't be exclusively indentified just by the XRD patterns,[53] and hence XPS was used for further characterization, as the core-electron lines of ferrous and ferric ions can both be detectable and distinguishable in XPS.[54] In the XPS spectrum of the as-prepared product (Figure 2b), no shake-up satellite structure (characteristic of Fe_2O_3) is found, and the photoelectron peaks at 710.8 and 724.2 eV match well with the characteristic doublet of Fe $2p_{3/2}$ and $2p_{1/2}$ core-level spectrum of Fe_3O_4.[55] The XPS analysis for Fe further confirms that the nanoparticles stuck on the surface of sepiolite are magnetite. However, when no sepiolite is added, the same experimental conditions lead to magnetite nanoparticles (Figure S1a and b in supporting information). SEM and TEM analyses show that obvious aggregation of magnetite nanoparticles occurs (Figure S1c and d).

The nitrogen adsorption/desorption isotherm and the BJH pore diameter distribution of raw sepiolite and modified sepiolite are shown in Figure 3. It can be seen that both raw sepiolite and modified sepiolite show an IV type N_2 adsorption isotherm with an evident hysteresis loop, suggesting the presence of mesopores in both materials.[40] The pore size distributions of the raw sepiolite (Figure 3a inset) and modified sepiolite (Figure 3b inset), determined from the adsorption branch of the isotherms, distribute within the range of 2-50 nm. The BET surface area and total pore volume are 256.5 m^2/g and 0.47 cm^3/g for raw sepiolite, and 155.9 m^2/g and 0.564 cm^3/g for sepiolite-supported magnetite nanoparticles, respectively. The surface area decrease of sepiolite-magnetite composite, compared with raw sepiolite, could attribute to the formation of magnetite nanoparticles on the raw sepiolite surface.

From these results, it can be concluded that sepiolite-supported magnetite nanoparticles with good dispersion are successfully harvested by a facile microwave reflux method. In the formation process of sepiolite-supported magnetite, Fe^{2+} and Fe^{3+} ions are firstly adsorbed on the sepiolite fibers owing to its high specific surface area, electrostatic attraction, and/or ion-exchange occurs with Mg^{2+} in sepiolite,[33,56] then form magnetite nanoparticles on the surface of sepiolite under microwave irradiation conditions. Sepiolite nanofibers have been successfully prepared under microwave condition.[57] In particular, we found that the raw

sepiolite can be heated under microwave irradiation, indicating that it is a microwave susceptor. As such, when sepiolite was irradiated by microwave, local hot spots can be created on the solid–liquid interfaces (i.e., the effect of hot spots),[46] which will enhance the interactions between sepiolite and magnetite nanoparticles. Meanwhile, the dissolved charged ions oscillate back and forth with high frequency under the influence of the MW field, leading to the formation of the strong binding sepiolite-supported magnetite nanoparticles with good dispersion. This was supported by our comparative experiments employing conventional oil bath heating reflux method. When the synthesis process was performed by oil bath heating reflux method at 200 ^{o}C for 20 min and 1 h, the SEM results show that the magnetite nanoparticles exhibit poor dispersibility on sepiolite, and obvious aggregates separated from sepiolite could be observed (Figure S2). In this regard, the present method is an efficient, simple, and time-saving route, and is potentially suitable for large-scale preparation.

3.2 Removal of Cr(VI) by the sepiolite-supported magnetite nanoparticles

In order to study the removal behavior of sepiolite-magnetite composite (SSM-1) to low concentration Cr(VI), the concentration of Cr(VI) was set as 2×10^{-5} mol/L (ca. 1.0 mg/L). As has been reported by other investigations, the removal of Cr(VI) by magnetite or nZVI is a coupled reduction sorption process, the removal mechanism of Cr(VI) are generally believed to involve adsorption of Cr(VI) on adsorbent surface where electron transfer takes place and then Cr(VI) is reduced to Cr(III) with the oxidation of Fe^{0} or Fe^{2+} to Fe^{3+}, subsequently, a part of Cr(III) precipitates as Cr^{3+} hydroxides and/or mixed Fe^{3+}/Cr^{3+} (oxy)hydroxides, and pH plays an important role in the Cr(VI) removal.[1,2,9,58] Thus, the pH-dependent experiments were first carried out at initial pHs from 2.0 to 11.0, mass of adsorbent/volume of solution (M/V) ratio of 50 mg/50 mL (i.e., adsorbent concentration is 1.0 g L^{-1}), temperature 293 K, and agitation time 24 h. As shown in Figure 4a, the final Cr(VI) removal has nearly no changes in the pH range 3.0 to 5.0, and then declines from 100% to 0 when the initial pH increases from 5.0 to 11.0, indicating that low pH values favor Cr (VI) removal. It is well known that surface charge of adsorbent is neutral at the point of zero charge (PZC), and adsorbent surface is positively charged below the pHzpc. The pHzpc of magnetite and sepiolite are about 6.5,[9] 7.4,[33] respectively. In addition, $HCrO_4^-$ and CrO_4^{2-} are the main species of Cr (VI) under

current conditions (i.e., the concentration of Cr(VI) solution is below 1 g/L and pH ranges from 2.0 to 11.0).[59] Therefore, the high Cr(VI) uptakes at low pH values can be attributed to the strong electrostatic attraction between the Cr(VI) oxyanions and the positive charged surface of the adsorbent. However, as the pH increases, the surface positive charges of the adsorbent decreases. As a result, the electrostatic attraction between negatively charged Cr(VI) species and the adsorbent will decrease, leading to the lowering uptake of Cr(VI) ions. On the other hand, a passivation layer, composed of maghemite, goethite, and/or $Fe_{1-x}Cr_xOOH$, may form on the magnetite surface at high pHs, and the reduction of Cr(VI) is usually limited.[9] The chromium uptake at pH 2.0 is lower than that at pH 3.0 (e.g., Figure 4a), which can be attributed to partial dissolution of magnetite nanoparticles, and partial decomposition of sepiolite, as the dissolution of sepiolite occurs below pH 3.0.[34] Moreover, the relationship between the Cr (VI) removal efficiency and final pH also exhibits that the final pH values greatly raise after the complete removal of Cr(VI) (Figure S3). This can be ascribed to the adsorption of H^+ ions onto sepiolite in the composite adsorbent, lowering the number of H^+ ions remaining in the solution. As a result, the higher final pHs were achieved.[34] The experiments above suggest that this adsorbent is suitable for the treatment of low level Cr(VI)-containing acidic wastewater (not lower than pH 3.0) from electroplating, mining, or leather tanning facilities over a wide pH range.[5]

The effect of contact time on the removal of Cr(VI) was investigated at pH 3.0, Cr(VI) concentration 1.0 mg/L, the studied contact times were 2, 6, 12, and 24 h. Figure 4b shows the Cr(VI) removal by SSM-1as a function of time, from which one can find that a very rapid removal of Cr(VI) in the first 2 h, about 94% of Cr(VI) is removed, and the concentration of residual Cr(VI) (ca. 0.05 mg/L) is under the EPA MCL limit level of Cr (i.e., 0.1 mg/L).[3] When the contact time prolongs to 12 h, nearly all Cr(VI) is removed, and the residual Cr(VI) is ca. 0.004 mg/L, far below the EPA MCL limit. The result suggests that the low concentration of Cr(VI) can be removed completely by the sepiolite-supported magnetite nanoparticles in short time.

Figure 4c displays the effect of mass of adsorbent/volume of solution (M/V) ratio on the removal of Cr(VI) (pH 3.0, contact time 24 h). The initial Cr(VI) concentration was increased to 10.78 mg/L, while the M/V ratio varied from 0.5 to 3 g/L. The removal efficiency of Cr(VI)

(the black solid line) increases with the increase in M/V ratio, when the M/V ratio is 1 g/L, nearly 80% of Cr(VI) is removed. After that, the removal efficiency increases slowly. The Cr(VI) is almost removed completely, as the M/V ratio reaches 2.5 g/L. The obtained results suggest that increasing the M/V ratio leads to an almost complete removal of Cr(VI), even the initial concentration of Cr(VI) is expanded to ten times, indicating this adsorbent is also useful for the treatment of high concentration Cr(VI). However, the removal capacity of the adsorbent (the red dash line) decreases with the increase in adsorbent concentration, when the adsorbent concentration exceeds 1.0 g/L. This may be because the aggregation of the magnetic adsorbent occurs at high adsorbent concentration, and hence limiting the removal capacity.

In addition, the effect of Cr(VI) concentration-dependence on the capacity of adsorbent was also investigated. As shown in Figure 4d, the maximum removal capacity of the adsorbent is found to be 9.3 mg/g for Cr(VI) at pH 3.0. To further assess the Cr(VI) removal ability of the SSMNPs, the amount of Cr(VI) adsorbed per unit mass (g) of magnetite was calculated based on the content of the loaded Fe_3O_4 (Table 1) and the values of $qe_{exp.}$(9.3 mg/g). The maximum removal capacity of Cr(VI) by SSM-1 is ca. 33.4 mg/g per unit mass (g) of magnetite. This value is higher than those of previously reported modified magnetite, such as PEG-4000 coated magnetite,[19] montmorillonite-supported magnetite nanoparticles,[28] and humic acid coated magnetite (HA-Fe_3O_4),[60] but lower than diatomite-supported magnetite nanoparticles prepared by common chemical co-precipitation method,[29] nanostructured Fe_3O_4 micron-spheres obtained by annealing hydrothermally formed $FeCO_3$ spheres in argon,[61] and cellulose derived magnetic mesoporous carbon nanocomposite,[62] as summarized in Table 2. However, taking into account of the facile, fast and efficient synthesized method, the microwave-assisted sepiolite-supported magnetite nanoparticles still have advantages in wastewater treatment applications.

Figure 4e shows the effect of magnetite loading on the removal capacity of Cr(VI). It is found that by increasing the magnetite loading from 16.37% (SSM-2) to 27.83% (SSM-1), the removal capacity (per unit mass of magnetite) increases: from 16.1 to 33.4 mg/g. However, as the magnetite loading is increased to 38.35% (SSM-3), the removal capacity of Cr(VI) decreases to 23.2 mg/g. The observed behavior can be attributed to the fact that the

aggregation of nanoparticles occurs with the increase of magnetite loading. As a result, the removal capacity of adsorbent is limited. The aggregation phenomenon is verified by the TEM image of SSM-3 (Figure S4).

The repeated availability of adsorbent after many cycles is quite crucial for the practical application. A simple regeneration test was conducted to evaluate the reusability of sepiolite-supported magnetite nanoparticles. As the Cr(VI) removal by magnetite is a irreversible coupled reduction sorption process rather than a simple physical sorption process, Cr-loaded adsorbent was used for the reusability test directly after rinsed by deionized water and dried under vacuum in our case. According to the recycling experiments of SSM-1 in the low concentration Cr(VI) (1.0 mg/L) removal (Figure 4f), we find that the removal efficiency does not show significant changes. After the second cycle, about 91 % of Cr(VI) is removed, and the concentration of residual Cr(VI) (ca. 0.093 mg/L) is under the EPA MCL limit level, with satisfied removal efficiency (80%) even in the fifth round, indicating that this adsorbent is valid for at least five cycles. The result also reflects that the removed Cr is not easily leached out from the adsorbent, this is real critical for the environment applications.

Moreover, the magnetite nanoparticles anchored tightly onto the rod-like sepiolite are not easily adsorbed to the cell membrane or wrapped by bacteria, and the introduction of clay as support material can effectively immobilize iron ions (e.g., Fe^{2+}, Fe^{3+}), which could cause cytotoxicity through Fenton reaction.[22,26] After the treatment with 10.4 mg/L of Cr(VI) for 24 h at pH 3.0 by unsupported magnetite nanoparticles, the concentration of Fe is ca. 82.45 mg/L. However, in SSMNPs treatment, the Fe concentration is only ca. 1.97 mg/L, much fewer Fe^{3+} ions are detected, even taking into account of the magnetite loading. This may be attributed to the adsorption of Fe^{3+} by sepiolite. The observations indicate that the introduction of sepiolite as a support material in magnetite water treatment systems can effectively immobilize Fe^{3+}. In this context, the magnetite nanoparticles stuck to the sepiolite could reduce the toxic effects of magnetic nanoparticles.

In short, the magnetite nanoparticles supported on rod-like sepiolite could balance the effects on their reactivity, capacity, reusability and biocompatibility, and taking into account of the facile fabrication method and possibility of magnetic separation of adsorbent with water, this adsorbent has real potential application in the treatment of low level acid

Cr(VI)-containing wastewater.

3.3 Mechanism of the Cr(VI) removal by sepiolite-supported magnetite nanoparticles

In order to understand the roles of sepiolite and magnetite nanoparticles in the sepiolite-magnetite composite during the Cr(VI) removal process, the removal abilities to Cr(VI) and Cr(Ⅲ) of raw sepiolite and unsupported magnetite nanoparticles (MNPs) were investigated at pH 3.0, respectively. Figure 5a depicts the removal capacities of raw sepiolite toward Cr(VI) and Cr(□), from which one can find that the adsorption of raw sepiolite to Cr(VI) is negligible, whereas the adsorption to cation Cr(Ⅲ) is ca. 0.7 mg/g. The significant difference is closely related to the surface charge of sepiolite and the predominant species of Cr(VI) at the final pH of the solution.[34] However, the removal capacities toward Cr(VI) and Cr(Ⅲ) of MNPs is ca. 22 mg/g and 8.4 mg/g, respectively (Figure 5b). Furthermore, after the introduction of sepiolite as support material, the Cr(VI) removal capacity of magnetite (SSM-1) is increased to 33.4 mg/g, about 50% higher than that of MNPs (ca. 22 mg/g). Combined with these results, it can safely concluded that in the sepiolite-magnetite composite, the nanoscale magnetite plays a crucial role in the removal of Cr(VI), whereas the sepiolite could disperse magnetite and prevent them from aggregation. Hence, the removal ability to Cr(VI) is enhanced after the magnetite nanoparticles are supported on sepiolite.

For further unveiling the mechanism of the removal of Cr(VI) by SSMNPs, a wide range techniques, including TEM, EDX, XRD and XPS, were used to characterize the adsorbent after the Cr(VI) removal. Figure 6a and b display the TEM images of SSM-1 after the removal of Cr(VI) (i.e., Cr-loaded SSM-1) (pH 3.0, initial Cr(VI) concentration 42 mg/L, 24 h), it is evident that much more precipitates can be observed on the surface of adsorbent, suggesting that the removed Cr(VI) may precipitate on the adsorbent surface, the element of Cr was also detected by the EDX (e.g., Figure 6b inset). The XPS was utilized to determine the oxidation state of Cr and Fe in Cr-loaded SSM-1and Cr-loaded MNPs. As shown in Figure 6c, the Cr2p XPS spectra of Cr-loaded SSM-1 appear at around 577 eV (typical peak of Cr(Ⅲ)), indicating that the adsorbed Cr(VI) is reduced to Cr(Ⅲ) by a heterogeneous redox process.[29,63] Due to the low content of Cr in Cr-loaded SSM-1, and the influence of sepiolite, the chromium signals in Cr-loaded SSM-1 is not evident as that in Cr-loaded MNPs. The Cr2p

spectrum in Cr-loaded MNPs display obvious two peaks at 577.2 and 586.3 eV, typical peaks of Cr(III), and no typical peaks of Cr(VI) are detected, confirming that the adsorbed Cr(VI) has been reduced into Cr(III) by magnetite (Figure 6c). Moreover, the binding energies and line structures of Cr are similar to $Cr(OH)_3$,[64-66] indicating that the removed Cr(VI) may exist as the form of $Cr(OH)_3$. The formation of $Cr(OH)_3$ may be due to the pH increase in the final solution after the removal of Cr(VI), and the low solubility product of $Cr(OH)_3$ (the Ksp of $Cr(OH)_3$ is 6.3×10^{-31}). Besides, in our experiment, the peak belongs to $Cr(OH)_3$ (JCPDS: 12-0241) appears in the XRD pattern of Cr-loaded magnetite (Figure 7), further confirming the existence of $Cr(OH)_3$. Figure 6d shows the XPS spectra of Fe in Cr-loaded SSM-1 and Cr-loaded MNPs. Both the Fe2p XPS spectra of SSM-1 and MNPs after the Cr(VI) removal show a oxidized state, as the characteristic of the Fe2p3/2 and Fe2p1/2 peaks center at ca. 711.0 and 724.8 eV, while the peaks are at ca. 710.5 and 724 eV in MNPs (Figure S1b), and ca. 710.8 and 724.2 eV in SSM-1 (Figure 2b), respectively. This result indicates that the Fe^{2+} in magnetite is partially oxidized into Fe^{3+} during the Cr(VI) reduction proces.[67] The increase of the binding energy of Fe was also suggested as an indication of the substitution of Cr^{3+} for Fe^{3+} in magnetite, due to the similar ionic radius of Fe^{3+} and Cr^{3+} (0.067nm for Fe^{3+} and 0.065nm for Cr^{3+}).[29,60,63] Generally, during the Cr(VI) removal processes, the Cr(VI) oxyanions are first adsorbed on the positive charged adsorbent surface, due to the strong electrostatic, then the high toxicity Cr(VI) is reduced into less toxicity Cr(Ⅲ) by structural Fe(II) in magnetite, while the structural Fe(II) is oxidized into Fe(III), and $Cr(OH)_3$ is finally formed due to raising pH.

Non-linear regression analysis of three isotherms, Langmuir, Freundlich and Redlich-Peterson, has been applied to the sorption data presented in this work. The applicability of the isotherm models to the sorption behavior was studied by judging the correlation coefficients, R^2. As it is known, Langmuir model assumes uniform adsorption on the surface and is valid for a monolayer sorption with a homogeneous distribution of the sorption sites and sorption energies. Freundlich isotherm can be used to describe the sorption on a heterogeneous surfaces as well as a multilayer sorption. Redlich-Peterson isotherm is a combination of Langmuir and Freundlich model, i.e., it approaches the Freundlich model at higher concentrations, while it is in accordance with the Langmuir equation at lower

concentrations. Figure 8 depicts the nonlinear plots of the comparison of the applied isotherms, and isotherm parameters are summarized in Table 3. Figure 8 and the values of the correlation coefficient (R^2) listed in Table 3 unambiguously reveal that the Langmuir equation and Redlich-Peterson isotherm give better interpretations of the experimental data than Freundlich, and the Redlich-Peterson isotherm is the most suitable model for the adsorption of Cr(VI).

4 Conclusions

In summary, SSMNPs with good dispersion prepared via a microwave irradiation technique show high removal efficiency, and much more significant adsorption capacity (33.4 mg/g) than that of the unsupported magnetite nanoparticles (22 mg/g) to low concentration Cr(VI). The removal of Cr(VI) by the SSNMPs involves an electrostatic attraction, followed by a reduction process of high toxicity Cr(VI) to less toxicity Cr(Ⅲ), and the subsequent surface precipitation of Cr(III) in the forms of $Cr(OH)_3$, meanwhile the Fe^{2+} in magnetite is oxidized into Fe^{3+}. In the system of magnetite-sepiolite composite, magnetite plays the main role in the removal and reduction of Cr(VI), while sepiolite as a support matrix, could not only disperse magnetite nanoparticles and prevent them from aggregation, thereby increasing the removal capacity to Cr(VI), but also effectively immobilize Fe^{3+} in the final solution, reducing the toxic effects of magnetite nanoparticles. Non-linear regression analysis reveals that the adsorption data fit well with the Redlich-Peterson isotherm model. The microwave-assisted synthetic method is efficient, simple, time-saving, and suitable for large-scale preparation. Taking into account of the possibility of magnetic separation of adsorbent with water, the SSMNPs can effectively remove heavy metals from aqueous solutions..

Acknowledgements

This work was partially supported by the Chinese Ministry of Science and Technology (No.

2014CB846003), the Natural Science Foundation of China (No. 41172049), and the Specialized Research Fund for the Doctoral Program of Higher Education (No. 20133402130007).

Supporting Information Available

The XRD, XPS spectrum of Fe, SEM, and TEM image of the product prepared by microwave-assisted method without sepiolite (Figure S1), TEM images of sepiolite-supported magnetite nanoparticles prepared by oil method for 20 min and 1 h (Figure S2), the relationship between the Cr (VI) removal efficiency and final pH (Figure S3), and TEM image of SSM-3 (Figure S4) are shown.

References

(1) J. Hu, G. H. Chen, and I. M. C. Lo, *Water Res.*, 2005, **39**, 4528-4536.

(2) L. Dupont and E. Guillon, *Environ. Sci. Technol.,* 2003, **37***,* 4235-4241.

(3) E. A. Ayuso, A. G. Sanchez, and X. Querol, *Water Res.,* 2003, **37**, 4855-4862.

(4) E. Kaprara, N. Kazakis, K. Simeonidis, S. Coles, A. I. Zouboulis, P. Samarase and M. Mitrakas, *J. Hazard. Mater.,* 2015, **281**, 2-11.

(5) D. H. Park, Y. S. Yun, J. H. Jo and J. M. Park, *Ind. Eng. Chem. Res.,* 2006*,* **45***,* 5059-5065.

(6) Y. M. Shi, X. H. Du, Q. J. Meng, S. W. Song and Z. T. Sui, *J. Iron. Steel. Res. Int.,* 2007, **14***,* 12-15.

(7) Y. J. Cheng, F. B. Yan, F. Huang, W. S. Chu, D. M. Pan, Z. Chen, J. S. Zheng, M. J. Yu, Z. Lin and Z. Y. Wu, *Environ. Sci. Technol.,* 2010, **44**, 6357-6363.

(8) W. Z. Liu, F. Huang, Y. J. Wang, T. Zou, J. S. Zheng and Z. Lin, *Environ. Sci. Technol.,* 2011, **45**, 1955-1961.

(9) Y. T. He and S. J. Traina, *Environ. Sci. Technol.,* 2005, **39**, 4499-4504.

(10) R. R. Patterson, S. Fendorf and M. Fendorf, *Environ. Sci. Technol.,* 1997, **31**, 2039-2044.

(11) G. Qin, M. J. Mcguire, N. K. Blute, C. Seidel and L. Fong, *Environ. Sci. Technol.,* 2005, **39**, 6321-6327.

(12) M. L. Peterson, A. F. White, G. E. Brown and G. A. Parks, *Environ. Sci. Technol.,* 1997, **31**, 1573-1576.

(13) T. Kendelewicz, P. Liu, C. S. Doyle and G. E. Brown, *Surf. Sci.,* 2000, **469**, 144-163.

(14) J. Farrell, W. D. Bostick, R. J. Jarabek and J. N. Fiedor, *Environ. Sci. Technol.,* 1999, **33**, 1244-1249.

(15) D. M. Singer, S. M. Chatman, E. S. Ilton, K. M. Rosso, J. F. Banfield and G. A. Waychunas, *Environ. Sci. Technol.,* 2012, **46**, 3821-3830.

(16) H. A. Wiatrowski, S. Das, R. Kukkadapu, E. S. Ilton, T. Barkay and N. Yee, *Environ. Sci. Technol.,* 2009, **43**, 5307-5313.

(17) J. T. Nurmi, P. G. Tratnyek, V. Sarathy, D. R. Baer, J. E. Amonette, K. Pecher, C. Wang, J. C. Linehan, D. W. Matson, R. L. Penn and M. D. Driessen, *Environ. Sci. Technol.,* 2005,

39, 1221-1230.

(18) M. Rivero-Huguet and W. D Marshall, *J. Hazard. Mater.,* 2009, **169**, 1081-1087.

(19) Y. F. Shen, J. Tang, Z. H. Nie, Y. D. Wang, Y. Ren and L. Zuo, *Bioresource Technol.,* 2009, **100**, 4139-4146.

(20) A. R. Petosa, D. P. Jaisi, I. R. Quevedo, M. Elimelech and N. Tufenkji, *Environ. Sci. Technol.,* 2010, **44**, 6532-6549.

(21) M. Auffan, W. Achouak, J. Rose, M. Roncato, C. Chanéac, D. T. Waite, A. Masion, J. C. Woicik, M. R. Wiesner and J. Bottero, *Environ. Sci. Technol.,* 2008, **42***,* 6730-6735.

(22) S. C. N. Tang and I. M. C. Lo, *Water Res.,* 2013, **47**, 2613-2632.

(23) S. M. Ponder, J. G. Darab and T. E. Mallouk, *Environ. Sci. Technol.,* 2000, **34**, 2564-2569.

(24) L. Hoch, E. Mack, B. Hydutsky, J. Hershman, J. Skluzacek and T. Mallouk, *Environ. Sci. Technol.,* 2008, **42**, 2600-2605.

(25) H. Jabeen, V. Chandra, S. Jung, J. W. Lee, K. S. Kim and S. B. Kim, *Nanoscale*, 2011, **3***,* 3583-3585.

(26) Y. M. Li, J. F. Li and Y. L. Zhang, *J. Hazard. Mater.,* 2012, **227-228**, 211-218.

(27) Ç. Üzüma, T. Shahwana, A. E. Eroğlua, K. R. Hallamb, T. B. Scottb and I. Lieberwirth, *Appl. Clay Sci.,* 2009, **43**, 172-181.

(28) P. Yuan, M. Fan, D. Yang, H. He, D. Liu, A. Yuan, J. Zhu and T. Chen, *J. Hazard. Mater.,* 2009, **166**, 821-882.

(29) P. Yuan, D. Li, M. D. Fan, D. Yang, R. Zhu, F. Ge, J. X. Zhu and H. P. He, *J. Hazard. Mater.,* 2010, **173**, 614-621.

(30) C. Y. Wan and B. Q. Chen, *Nanoscale,* 2011, **3***,* 693-700.

(31) N. García, J. Guzmán, E. Benito, A. Esteban-Cubillo, E. Aguilar, J. Santarén and P. Tiemblo, *Langmuir.* 2011, **27**, 3952-3959.

(32) M. Doğan, Y. Turhan, M. Alkan, H. Namli, P. Turan and Ö. Demirbaş, *Desalination,* 2008, **230**, 248-268.

(33) S. Lazarević, I. Janković-Častvan, D. Jovanović, S. Milonjić, D. Janaćković and R. Petrović, *Appl. Clay Sci.,* 2007, **37**, 47-57.

(34) V. Marjanović, S. Lazarević, I. Janković-Častvan, B. Potkonjakć, Đ. Janaćković and R.

Petrović, *Chem. Eng. J.,* 2011, **166**, 198-206.

(35) A. Tabak, E. Eren, B. Afsin and B. Caglar, *J. Hazard. Mater.,* 2009, **161**, 1087-1094.

(36) N. Güngör, S. Işçi, E. Günister, W. Mišta, H. Teterycz, R. Klimkiewicz, *Appl. Clay Sci.,* 2006, **32**, 291-296.

(37) S. Suárez, J. M. Coronado, R. Portela, J. C. Martín, M. Yates, P. Avila and B. Sánchez, *Environ. Sci. Technol.,* 2008, **42**, 5892-5896.

(38) W. G. Xu, S. F. Liu, S. X. Lu, S. Y. Kang, Y. Zhou and H. F. Zhang, *J. Colloid Interf. Sci.,* 2010, **351**, 210-216.

(39) Q. W. Zhu, Y. H. Zhang, F. Z. Lv, P. K. Chu, Z. F. Ye and F. S. Zhou, *J. Hazard. Mater.,* 2012, **217-218**, 11-18.

(40) H. C. Liu, W. Chen, C. Liu, Y. Liu and C. L. Dong, *Microporous Mesoporous Mater.,* 2014, **194**, 72-78.

(41) H. C. Liu and W. Chen, *RSC Adv.* 2015, **5**, 27034-27042.

(42) R. Gedye, F. Smith, K. Westaway, A. Humera, L. Baldisera, L. Laberge and L. Rousell, *Tetrahedron Lett.,* 1986, **27**, 279-282.

(43) R. Giguere, T. L. Bray, S. M. Duncan and G. Majetich, *Tetrahedron Lett.,* 1986, **27**, 4945-4948.

(44) V. K. Tyagi and S. L. Lo, *Renewable Sustainable Energy Rev.,* 2013, **18**, 288-305.

(45) K. J. Rao, B. Vaidhyanathan, M. Ganguli and P. A. Ramakrishnan, *Chem. Mater.,* 1999, **11**, 882-895.

(46) Q. Z. Yao, G. Jin and G. T. Zhou, *Mater. Chem. Phys.,* 2008, **109**, 164-168.

(47) M. L. Li, Q. Z. Yao, G. T. Zhou and S. Q. Fu, *CrystEngComm,* 2010, **12,** 3138-3144.

(48) C. F. Mu, Q. Z. Yao, X. F. Qu, G. T. Zhou, M. L. Li and S. Q. Fu, *Colloids Surf., A.* 2010, **371**, 14-21.

(49) M. L. Li, Q. Z. Yao, G. T. Zhou, X. F. Qu, C. F. Mu, S. Q. Fu, *CrystEngComm,* 2011, **13**, 5936-5942.

(50) N. B. Milosavljevic, M. D. Ristic, A. A. Peric-Grujic, J. M. Filipovic, S. B. Strbac, Z. L. Rakocevic and M. T. Kalagasidis Krusic, *Colloid Surf. A,* 2011, **388**, 59-69.

(51) E. Ruiz-Hitzky, *J. Mater. Chem.* 2001, **11**, 86-91.

(52) X. F. Qu, G. T. Zhou, Q. Z. Yao and S. Q. Fu, *J. Phys. Chem. C,* 2010**, 114***,* 284-289.

(53) X. F. Qu, G. T. Zhou, Q. Z. Yao and S. Q. Fu, *J. Phys. Chem. C,* 2010**, 114***,* 8734-8740.

(54) I. D. Welsh and M. A. Sherwood, Phys. Rev. B: Con-dens. *Matter Mater. Phys.*, 1989, **40**, 6386-6392.

(55) T. Fujii, F. M. F. de Groot, G. A. Sawatzky, F. C. Voogt, T. Hibma and K. Okada, *Phys. Rev. B,* 1999, **59**, 3195-3202.

(56) X. P. Gu, X. D. Xie, X. B. Wu, G. C. Zhu, J. Q. Lai, K. Hoshino and J. W. Huang, *Eur. J. Mineral.,* 2013**, 25***,* 177-186.

(57) F. Wang, J. S. Liang, Q. G. Tang, C. Chen and Y. L. Chen, *Adv. Mater. Res. (Durnten-Zurich, Switz.),* 2012, **427**, 82-87.

(58) D. Mohana, C. and U. Pittman Jr., *J. Hazard. Mater.,* 2006, **137***,* 762-811.

(59) C. H. Weng, J. H. Wang and C. P. Huang, *Water Sci.Technol.,* 1997, **35**, 55-62.

(60) W. Jiang, Q. Cai, W. Xu, M. Yang, Y. Cai, D. D. Dionysiou and K. E. O'Shea, *Environ. Sci. Technol.,* 2014, **48**, 8078-8085.

(61) G. Liu, Q. Deng, H. M Wang, S. H. Kang, Y. Yang, D. H. L. Ng, W. P. Cai and G. Z. Wang, *Chem. Eur. J.,* 2012, **18**, 13418-13426.

(62) B. Qiu, H. Gu, X. Yan, J. Guo, Y. Wang, D. Sun, Q. Wang, M. Khan, X. Zhang, B. L. Weeks, D. P. Young, Z. Guo and S. Wei, *J. Mater. Chem. A,* 2014, **2**, 17454-17462.

(63) J. Manjanna and G. Venkateswaran, *Ind. Eng. Chem. Res.,* 2002, **41**, 3053-3063.

(64) A. R. Pratt and N. S. McIntyre, *Surf. Interface Anal.,* 1996, **24**, 529-530.

(65) X. Q. Li, J. S. Cao and W. X. Zhang, *Ind. Eng. Chem. Res.,* 2008, **47**, 2131-2139.

(66) M. C. Biesinger, C. Brown, J. R. Mycroft, R. D. Davidson and N. S. McIntyre, *Surf. Interface Anal.,* 2004, **36**, 1550-1563.

(67) M. V. Kuznetsov, O. D. Linnikov and I. V. Rodina, *Inorg. Mater.,* 2012, **48**, 169-175.

Figure captions

Figure 1. SEM and TEM images of sepiolite before (a) and after (b, c, d) modification by microwave-assisted method; inset of panel a: TEM image of the raw sepiolite; inset A of panel b: the magnetic property of the modified sepiolite; inset B of panel b: EDX spectra of the modified sepiolite; inset of panel d: high-resolution TEM image of the modified sepiolite.

Figure 2. (a) XRD patterns of raw sepiolite and modified sepiolite, (b) XPS spectrum of Fe in the modified sepiolite.

Figure 3. N_2 Adsorption/desorption isotherms and BJH pore diameter distributions (inset) of raw sepiolite (a), and modified sepiolite (b).

Figure 4. Effects of pH (a), contact time (b), adsorbent concentration (c), initial Cr(VI) concentration (d) and magnetite loading on the removal of Cr(VI) by SSM-1; (f) the repeated availability of SSM-1.

Figure 5. The removal capacity of raw sepiolite (a) and unsupported magnetite (b) to Cr(VI) and Cr(□).

Figure 6. TEM images (a, b) of Cr-loaded SSM-1, XPS spectra of Cr (c) and Fe (d) in Cr-loaded SSM-1 and Cr-loaded MNPs; inset of panel b: EDX spectra of Cr-loaded SSM-1.

Figure 7. XRD patterns of Cr-loaded SSM-1 and Cr-loaded MNPs.

Figure 8. Comparison of Freundlich, Langmuir and Redlich-Peterson isotherms for the Cr(VI) adsorption at pH 3.0 onto SSM-1 (a) and MNPs (b).

Table 1. Experimental conditions for typical samples

Sample NO.	System	Sepiolite	Magnetite loading
SSM-1	$FeCl_3 \cdot 6H_2O$ (0.27 g)/$FeCl_2.4H_2O$ (0.10 g)/sepiolite/EG (20 mL) + 0.16g NaOH/H_2O (5 mL)	0.25 g	27.83%
SSM-2	Same as sample 1	0.50 g	16.37%
SSM-3	Same as sample 1	0.125 g	38.35%
MNPs	Same as sample 1	-	-

Table 2. Cr(VI) removal capacities of various magnetite adsorbents

adsorbent sample	maximum adsorption capacity per unit mass of magnetite (mg/g)	initial pH	adsorbent dose (g/L)	Ref
PEG-4000 coated magnetite (12 nm)	23.12	4.0	5.0	19
magnetite (35 nm)	7.45	4.0	5.0	19
montmorillonite-supported magnetite nanoparticles	15.3	2.5	5.0	28
diatomite-supported magnetite nanoparticles	69.2	2.5	5.0	29
humic acid coated magnetite (HA-Fe_3O_4)	3.37	4.0	0.8	60
Nanostructured Fe_3O_4 Micron-Spheres	43.48	3.0	1.0	61
magnetic mesoporous carbon nanocomposite	293.8	2.5	1.0	62
sepiolite-support magnetite (SSM-1)	33.4	3.0	1.0	this work
unsupported magnetite	22	3.0	1.0	this work

Table 3. The Langmuir, Freundlich and Redlich–Peterson parameters for Cr(VI) adsorption on sepiolite-supported magnetite nanoparticles (SSM-1) and unsupported magnetite nanoparticles (MNPs)

Adsorbent	pH	Langmuir			Freundlich			Redlich–Peterson			
		K_L	b	R^2	K_F	n	R^2	K_R	a_R	β	R^2
SSM-1	3	8.98	6.73	0.987	5.86	6.84	0.855	89.54	11.14	0.96	0.995
MNPs	3	21.2	38.20	0.987	14.2	6.58	0.863	915.9	45.83	0.97	0.991

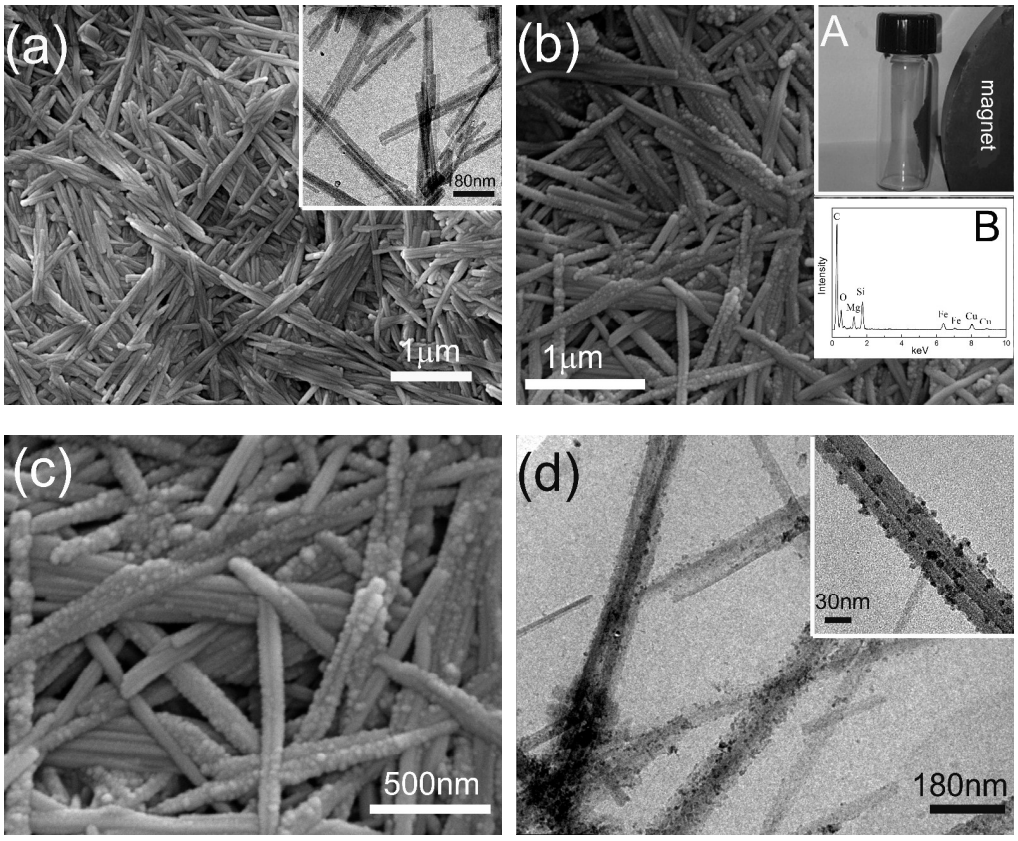

Fig. 1

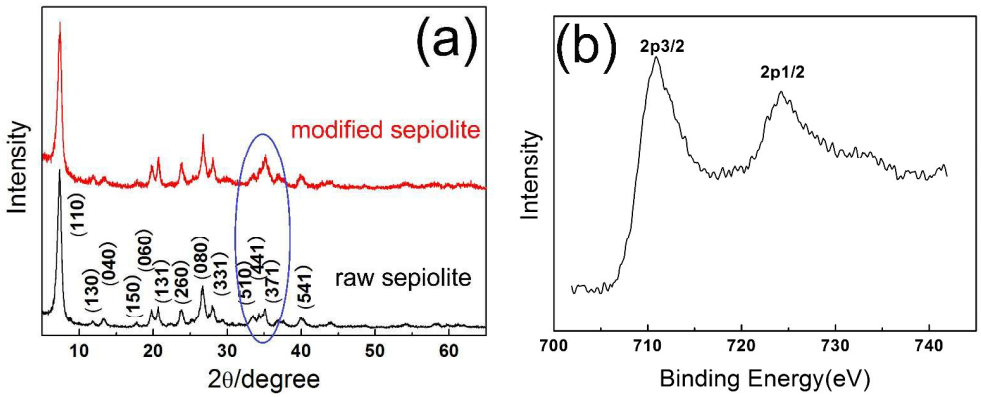

Fig. 2

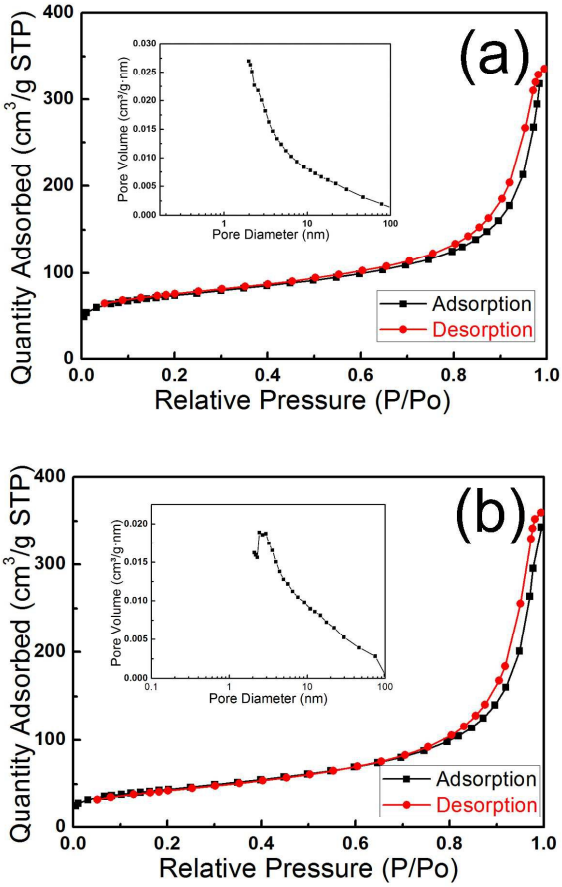

Fig. 3

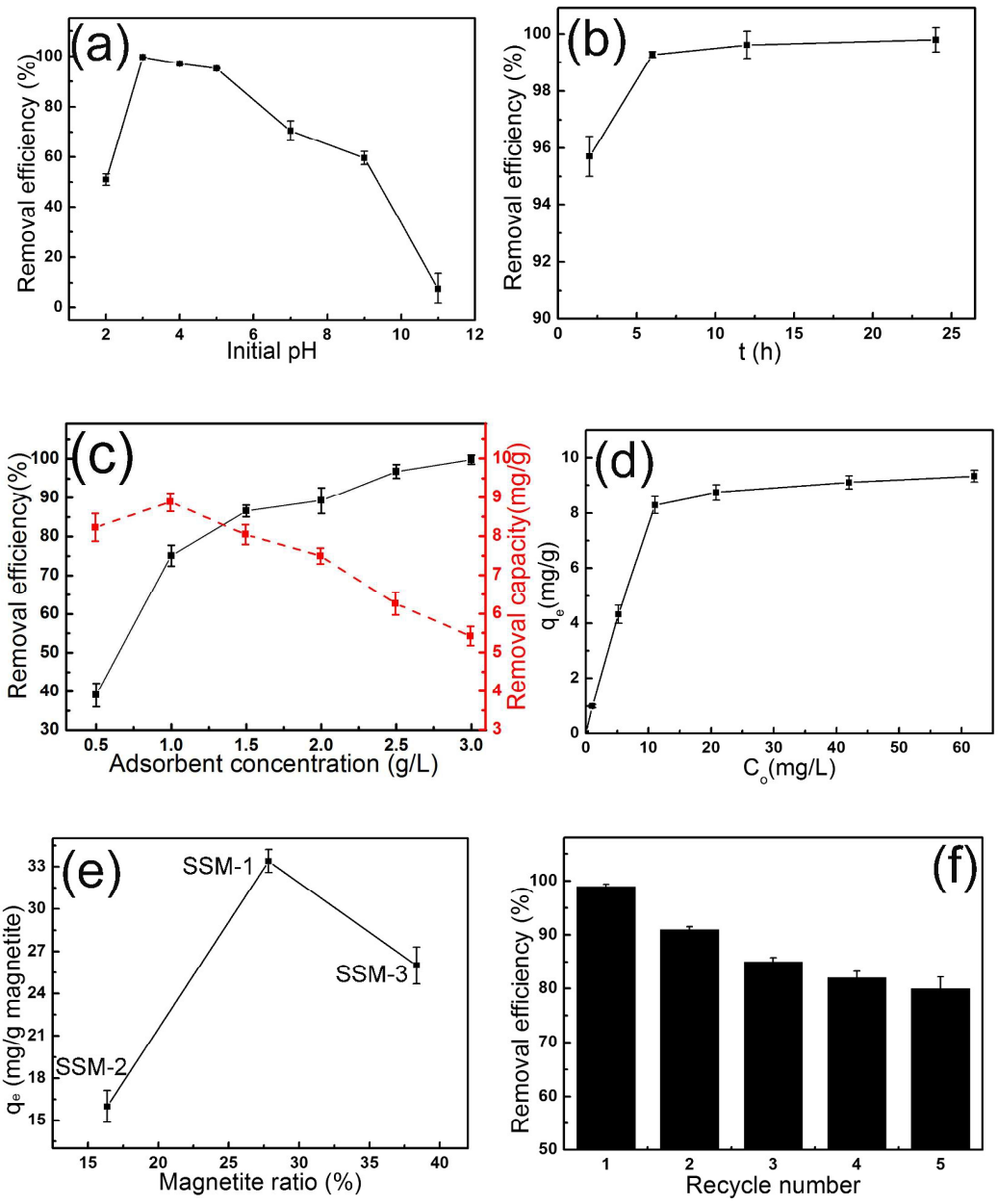

Fig. 4

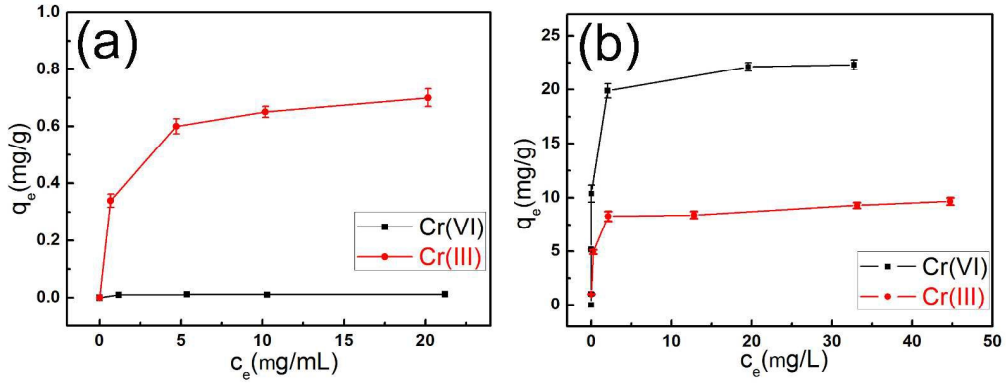

Fig. 5

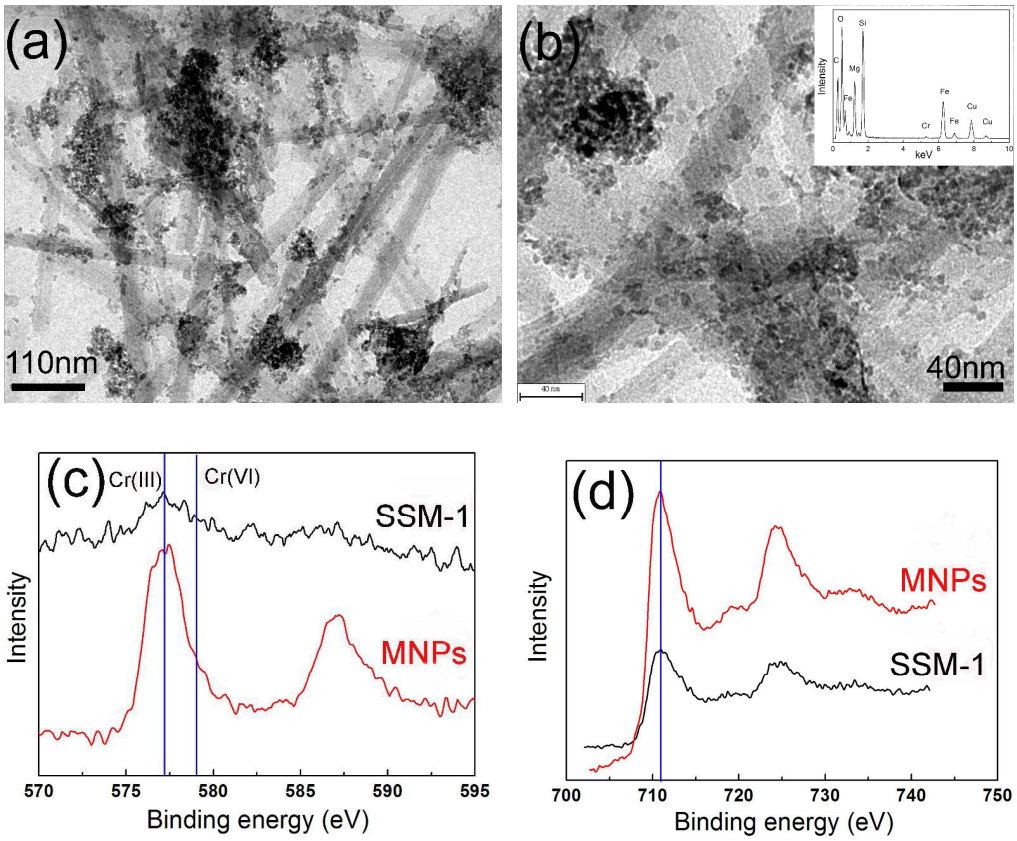

Fig. 6

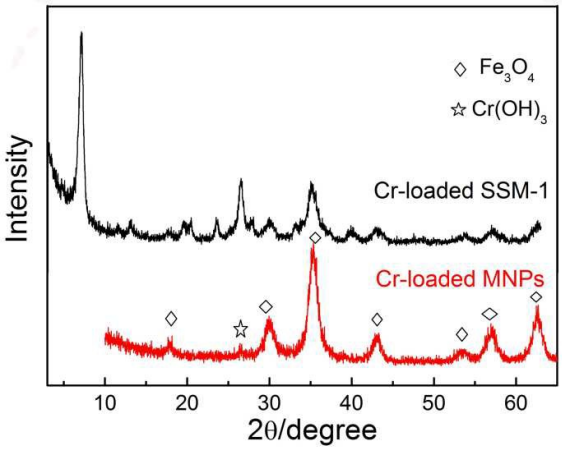

Fig. 7

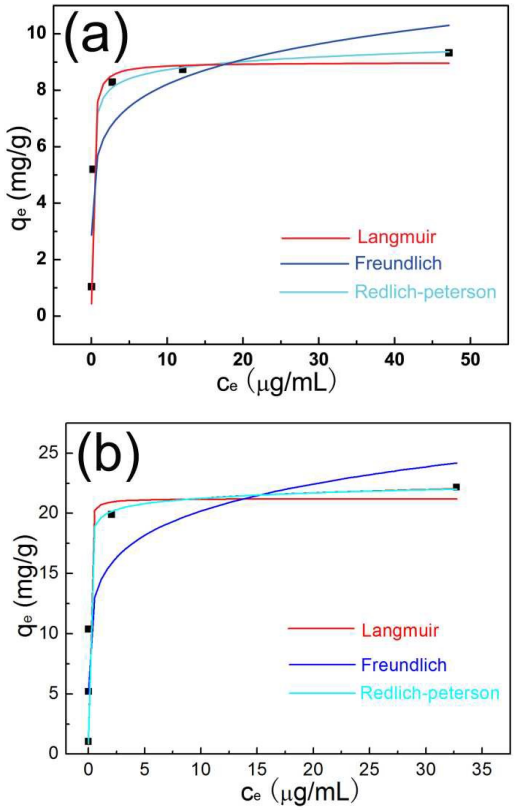

Fig. 8

Graphical abstract

Speiolite-nanomagnetite composite obtained by a facile microwave-assisted route can not only remove low concentrate of Cr(VI), but also effectively immobilize the secondary Fe^{3+} in the final solution.